Lamb shift multipolar analysis

Emmanuel Lassalle, Alexis Devilez, Nicolas Bonod, Thomas Durt, Brian Stout

Lamb shift multipolar analysis

Emmanuel Lassalle, Alexis Devilez, Nicolas Bonod, Thomas Durt, and Brian Stout*
Aix Marseille Univ, CNRS, Centrale Marseille, Institut Fresnel, Marseille, France
(Dated: April 5, 2018)

It is now well established that radiative decay of quantum emitters can be strongly modified by their environment. In this paper we present an exact — within the weak-coupling approximation — multipole expression to compute the Lamb (frequency) shift induced by an arbitrary set of resonant scatterers on a nearby quantum emitter, using multi-scattering theory. We also adopt a Quasi-Normal Mode description to account for the line shape of the Lamb shift spectrum in the near-field of a plasmonic nanosphere. It is then shown that the Lamb shift resonance can be blue-shifted as the size of the nanoparticle increases, suggesting that nanoparticles may be used to tune this resonant interaction. Finally, a realistic calculation of the Lamb shift is made for a dimer configuration.

I. INTRODUCTION

Control of the decay properties of quantum emitters *via* modifications of their local electromagnetic environment is being actively pursued due to the rich perspectives it offers for both fundamental and practical applications [1]. In the weak-coupling regime, the exponential decay in time of the excited state is characterized by the decay rate, for which it is well known that it can be either enhanced [2] or inhibited [3] by the local electromagnetic (EM) environment. With the convergence of communities such as near-field optical microscopy, semiconductors, plasmonics, and metamaterials, engineering the quantum vacuum allows tailoring the decay rate in unprecedented ways [4, 5]. A less often discussed effect of spontaneous emission is that the surrounding environment also induces level shifts of the excited atomic states, resulting in a frequency-shift for the emitted photons, in comparison with the bare resonance frequency. This is the so-called *Lamb shift*, which originally refered to level shifts of atoms in free space [6, 7], also called radiative frequency-shift or Casimir-Polder frequency-shift. This effect has been theoretically studied in the case of perfect reflectors [8], partially reflecting surfaces [9, 10] and photonic crystals [11–13]. Multipole formulas of the Lamb shift have been derived in the case of a dielectric microsphere without [14, 15] and with [16] absorption, and for dielectric or metallic prolate spheroids [17]. However, there is no such formulas in multi-scattering configurations, except in the case of two-dimensional photonic crystals [18].

In this article, we derive — using the generalized Mie theory [19, 20] — a multipole formula for the Lamb shift of a quantum emitter induced by an arbitrary set of scatterers. This formula is exact within the weak-coupling approximation and does not take into account non-local effects which come into play for emitter - particle distances below one nanometer [21].

Section II justifies the use of a classical formalism to study the Lamb shift induced by the presence of matter by showing, in the weak-coupling approximation, its equivalence to the fully quantum result. An exact multipole formula for the Lamb shift is then derived in section III and illustrated in section IV by computing the Lamb shift in the vicinity of a silver nanosphere, where we also show that the spectral line shape of the Lamb shift can be accounted for in the context of a "Quasi-Normal Mode" description. In section V, we study the influence of the nanoparticle's size on the environmentally induced Lamb shift, and we predict a displacement of the emitter's Lamb shift resonance as the size of the nanoparticle changes. Finally, as a practical calculation, we compute the Lamb shift in the case of a dimer nanoantenna.

II. ENVIRONMENTALLY INDUCED LAMB SHIFT

A. Classical approach

An excited two-level atom with transition frequency ω_0 and natural linewidth γ_0 can be modeled by a harmonically oscillating *point dipole*, whose electric dipole moment $\mathbf{p}(\mathbf{r}_0,t)$ obeys, in the case of *small damping* ($\gamma_0 \ll \omega_0$) [22]:

$$\frac{d^2\mathbf{p}(\mathbf{r}_0,t)}{dt^2}+\gamma_0\frac{d\mathbf{p}(\mathbf{r}_0,t)}{dt}+\omega_0^2\mathbf{p}(\mathbf{r}_0,t)=\frac{q^2}{m}\mathbf{E}_s(\mathbf{r}_0,t)\ , \quad (1)$$

where $\{\omega_0,\ \gamma_0,\ q,\ m\}$ are the characteristics of the classical dipole (the natural frequency of the oscillator, the damping constant in the *homogeneous* background, the charge and the mass respectively) and $\mathbf{E}_s(\mathbf{r}_0,t)$ is the field scattered by the environment at the dipole position $\mathbf{r}_0$. Adopting the following *ansatz*:

$$\begin{cases} \mathbf{p}(\mathbf{r},t)=\mathbf{p}_0e^{-\mathrm{i}\Omega t} \\ \mathbf{E}_s(\mathbf{r}_0,t)=\mathbf{E}_s(\mathbf{r}_0,\omega_0)e^{-\mathrm{i}\Omega t} \end{cases} \text{ where } \begin{cases} \Omega=\omega_0+\Delta\omega-\mathrm{i}\frac{\gamma}{2} \\ \Delta\omega=\omega-\omega_0 \end{cases}, \quad (2)$$

with γ and ω respectively indicating the new decay rate and resonance frequency, together with the *weak-coupling approximation* in a classical context,

$$\frac{q^2}{m}|\mathbf{E}_s| \ll \omega_0^2|\mathbf{p}|\ , \quad (3)$$

one finds the following expression for the frequency-shift of the light emitted by the dipole due to the environment

* brian.stout@fresnel.fr

[22]:

$$\left.\frac{\Delta\omega}{\gamma_0}\right|_{\omega_0} = -\frac{3\pi\epsilon_0\varepsilon_b}{k^3} \times \frac{1}{|\mathbf{p}_0|^2} \times \mathrm{Re}(\mathbf{p}_0^* \cdot \mathbf{E}_s(\mathbf{r}_0,\omega_0)) \ , \quad (4)$$

where $k = n_b(\omega_0/c)$ is the wave-number of the nonabsorbing homogeneous background medium of refractive index $n_b = \sqrt{\varepsilon_b}$. In this classical picture, one can see from Eq. (4) that the environment contribution to the frequency-shift is due to the dipole interacting with its own electric field scattered back by the environment.

To link this expression with the quantum one, one can derive the dipole fields using the *Green-function* formalism (for the sake of simplicity, we consider the dipole emitter to be in vacuum: $\varepsilon_b = 1$). The field produced at $\mathbf{r}$ by a *point* dipole located at $\mathbf{r}_0$ and with natural frequency ω_0 is [22]:

$$\mathbf{E}(\mathbf{r},\omega_0) = \omega_0^2\mu_0\overleftrightarrow{\mathbf{G}}(\mathbf{r},\mathbf{r}_0,\omega_0)\cdot\mathbf{p}_0 \ , \quad (5)$$

where $\overleftrightarrow{\mathbf{G}}$ denotes the dyadic Green tensor. By separating the Green tensor into an "unperturbed" $\overleftrightarrow{\mathbf{G}}_0$ plus a "scattering" $\overleftrightarrow{\mathbf{G}}_s$ contributions [22],

$$\overleftrightarrow{\mathbf{G}} = \overleftrightarrow{\mathbf{G}}_0 + \overleftrightarrow{\mathbf{G}}_s \ , \quad (6)$$

Eq. (4) can be cast in terms of the scattering Green tensor:

$$\left.\frac{\Delta\omega}{\gamma_0}\right|_{\omega_0} = -\frac{3\pi c}{\omega_0} \times \mathbf{u}_p \cdot \mathrm{Re}(\overleftrightarrow{\mathbf{G}}_s(\mathbf{r}_0,\mathbf{r}_0,\omega_0))\cdot\mathbf{u}_p \ , \quad (7)$$

with $\mathbf{u}_p$ being the unit vector in the direction of the dipole moment: $\mathbf{p}_0 = p_0\mathbf{u}_p$.

B. Quantum approach

In a quantum approach, the excited two-level atom is modeled by its state vector $|e\rangle$, and its interaction with the electromagnetic field is represented by an interaction Hamiltonian $\hat{H}_I$. The *weak-coupling approximation* in a quantum context consists of considering that the matrix elements of the interaction Hamiltonian are small compared to those of the non-interacting Hamiltonian $\hat{H}_0$. Therefore, the energy level shift ΔE of the excited atomic state is calculated by using the usual perturbation theory to second order in the perturbation $\hat{H}_I$. Besides, by using the fluctuation-dissipation theorem, one can show that the energy-shift of the first excited state $|e\rangle$ of bare frequency ω_0 is [10]:

$$\Delta E|_{\omega_0} = -\frac{\omega_0^2}{\pi\epsilon_0 c^2}\, p_i p_j\, \mathcal{P}\left[\int_0^{+\infty} \mathrm{d}\omega\, \frac{\mathrm{Im}\left(G_{ij}(\mathbf{r}_0,\mathbf{r}_0,\omega)\right)}{\omega-\omega_0}\right] , \quad (8)$$

where $\mathcal{P}$ denotes the principal value of the integral, $\mathbf{p} = \langle g|\,\hat{\mathbf{p}}\,|e\rangle$ ($\hat{\mathbf{p}}$ being the dipole moment operator and $|g\rangle$ the ground state vector) is the transition dipole matrix element, and G_{ij} is the previous classical Green tensor (let us note that the notation $\overleftrightarrow{\mathbf{G}}$ used in [10] is the field susceptibility that we call $\overleftrightarrow{\mathbf{F}}$, and which is related to the Green tensor by $\overleftrightarrow{\mathbf{F}}(\mathbf{r},\mathbf{r}',\omega) \leftrightarrow \omega^2\mu_0\overleftrightarrow{\mathbf{G}}(\mathbf{r},\mathbf{r}',\omega)$). By using the Kramers-Kronig relations for the Green tensor, and separating as previously the Green tensor into two contributions, one can cast the frequency-shift resulting from the energy level shift induced by the presence of matter, in the form:

$$\Delta\omega|_{\omega_0} = -\frac{\omega_0^2}{\hbar\epsilon_0 c^2}\, p_i p_j\, \mathrm{Re}\left((G_s)_{ij}(\mathbf{r}_0,\mathbf{r}_0,\omega_0)\right) + \mathrm{QC} \ . \quad (9)$$

Except for the non-resonant quantum correction term QC which is negligibly small [16], this expression has the same form as the classical formula provided that one normalizes by the quantum decay rate in free space

$$\gamma_0 = \frac{\omega_0^3|\mathbf{p}|^2}{3\pi\epsilon_0\hbar c^3} \ , \quad (10)$$

because the normalization eliminates the dependency on $\mathbf{p}$ and provides a safe link between quantum and classical formalisms.

Thus, in the *weak-coupling regime*, the quantum treatment gives the same result as the classical treatment when considering the normalized frequency-shift — that we will call Lamb shift in the following — *between the ground state and the first excited state* (to consider other atomic levels, the classical treatment and the two-level atom model fail, and one must refer to the general formula derived in [10]). Note that for an *absorbing* medium, characterized by an imaginary part of its permittivity, this equivalence still holds, because on one hand, in the classical approach developed in terms of the Green tensor, the permittivity can become complex, and in a quantum context, the link between the ground-state fluctuations of the electric field and the classical Green tensor remains the same [16, 23, 24].

III. MULTIPOLE FORMULA FOR THE LAMB SHIFT

Now we move to the derivation of the exact multipole formula for the Lamb shift induced by an arbitrary set of resonant scatterers on a nearby quantum emitter. One can see from Eq. (4) that the Lamb shift induced by the surrounding environment is embodied in the field scattered by the environment $\mathbf{E}_s$, which can be calculated from the scattering part $\overleftrightarrow{\mathbf{G}}_s$ of the total Green tensor through Eqs. (5) and (6). The determination of $\overleftrightarrow{\mathbf{G}}_s$ is thus the chief obstacle to the calculation of the Lamb shift. From a classical viewpoint, the scattering Green tensor $\overleftrightarrow{\mathbf{G}}_s$ must take into account the multiple scattering of the incident radiation from all the scatterers. Therefore, for the purpose of calculation, it is advantageous to express the scattering Green tensor in terms of the

multiple-scattering T-Matrix [25], where the T-Matrix is defined in operator notation as

$$\overleftrightarrow{\mathbf{G}}_s = \overleftrightarrow{\mathbf{G}}_0 \overleftrightarrow{\mathbf{T}} \overleftrightarrow{\mathbf{G}}_0 = \overleftrightarrow{\mathbf{G}}_0 \left(\sum_{i=1,j=1}^{N} \overleftrightarrow{\mathbf{T}}^{(i,j)} \right) \overleftrightarrow{\mathbf{G}}_0 \ , \qquad (11)$$

and has been split into N^2 operators $\overleftrightarrow{\mathbf{T}}^{(i,j)}$ (that represent all multiple-scattering events from a multiple-scattering viewpoint [19]), i and j being the particle labels, and N the total number of scatterers.

In order to calculate the $\overleftrightarrow{\mathbf{T}}^{(i,j)}$ operators, we will make use of the multipolar fields — also called multipolar modes or multipoles — which are a set of basis EM modes that are especially useful in describing EM scattering for particles with spherical symetries [26]. We will denote a multipolar field as $|\mathbf{\Psi}_{q,n,m}\rangle$, each mode being specified by three discrete numbers: q accounts for the parity of the field, and $q = 1$ for a magnetic mode and $q = 2$ for an electric mode; $n = 1, 2, ..., \infty$ and will be called the "multipolar order"; and $m = -n, ..., n$ and will be called the "orbital number". Explicit representations of these modes can be found in [26], and here the fields and operators will be expressed in the basis of the multipolar fields satisfying the outgoing boundary conditions (called the Hankel multipolar fields in [26]), that we will note $\mathbf{M}_{nm}(k\mathbf{r})$ for the magnetic modes ($q = 1$) and $\mathbf{N}_{nm}(k\mathbf{r})$ for the electric modes ($q = 2$) in the real space representation.

The $\overleftrightarrow{\mathbf{T}}^{(i,j)}$ operators are then expressed in the multipole basis [25]:

$$\overleftrightarrow{\mathbf{T}}^{(i,j)} = \sum_{q,q'=1}^{2} \sum_{n,n'=1}^{\infty} \sum_{m=-n}^{n} \sum_{m'=-n'}^{n'} |\mathbf{\Psi}_{q,n,m}\rangle \, T^{(i,j)}_{q,n,m;q',n',m'} \, \langle \mathbf{\Psi}_{q',n',m'}| \ , \qquad (12)$$

and can be calculated from the infinite dimensional $T^{(i,j)}$ matrices, that can be rendered finite by truncating the multipolar order n to some finite dimension n_{cut} (the choice of n_{cut} for which the summation with respect to the multipolar order n converges will depend on particle size and interaction strengths). Several methods exist for calculating the $T^{(i,j)}$ matrices, and we use the analytical balancing techniques detailed in [20] and implemented in an in-house code used for the numerical simulations of this article. Once the on-shell $T^{(i,j)}$ matrices have been determined, one can compute the expression of the electric field $\mathbf{E}_s(\mathbf{r}_0, \omega_0)$ scattered by the environment by employing Eq. (11) in Eqs. (6) and (5):

$$\mathbf{E}_s(\mathbf{r}_0, \omega_0) = \frac{\mathrm{i} p_0 k \omega_0^2}{\epsilon_0 c^2} \sum_{i,j=1}^{N} \left[[\mathbf{M}(k\mathbf{r}_i), \mathbf{N}(k\mathbf{r}_i)]^t T^{(i,j)} H^{(j,0)} f \right] \ , \qquad (13)$$

where $[\mathbf{M}, \mathbf{N}]$ is a column matrix composed of the $\mathbf{M}_{nm}$ and $\mathbf{N}_{nm}$ functions, f represents the dipolar source and denotes a column matrix containing the emitter coefficients in the multipole space, and $H^{(j,0)}$ is the irregular translation-addition matrix between the emitter position at $\mathbf{r}_0$ and the position of particle j (for more details, see the derivation of Eq. (19) in [25]).

Finally, the expression of $\mathbf{E}_s(\mathbf{r}, \omega_0)$ can be utilized in Eq. (4) to obtain the multipole expression for the normalized Lamb shift induced by the presence of N scatterers:

$$\frac{\Delta\omega}{\gamma_0} = 3\pi \times \mathrm{Im} \left(\sum_{i,j=1}^{N} f^t H^{(0,i)} T^{(i,j)} H^{(j,0)} f \right) \ . \qquad (14)$$

In the case of a single particle ($N = 1$), Eq. (14) takes the form:

$$\frac{\Delta\omega}{\gamma_0} = 3\pi \times \mathrm{Im} \left(f^t H^{(0,1)} t H^{(1,0)} f \right) \ , \qquad (15)$$

where t is the single-particle T-Matrix. In the case of a spherical Mie scatterer, t is a diagonal matrix composed of the Mie coefficients of the sphere (given in Appendix VII A), and Eq. (15) is then equivalent to expressions previously derived for a single sphere [15, 16]. Exact analytical expressions of the first two multipolar contributions to the Lamb shift can be found in Appendix VII B.

IV. MULTIPOLAR ANALYSIS

A. Multipole contributions to the Lamb shift

Let us first calculate the Lamb shift in the case of a silver nanosphere of radius $a = 20\,\text{nm}$ in vacuum ($n_b = 1$). Based on Eq. (15), we compute using an in-house code the Lamb shift of a quantum emitter radially oriented and located at a distance $d = 10\,\text{nm}$ from the nanoparticle, as a function of the bare transition wavelength $\lambda_0 = 2\pi c/\omega_0$ (black curve in Fig. 1). We analyze this Lamb shift spectrum by plotting separately the different multipolar contributions (plotted in colors in Fig. 1: $n = 1$ corresponds to the contribution of the dipolar mode, $n = 2$ to the contribution of the quadrupolar mode and so on). One can thus see that in the near-field of the nanoparticle, the total Lamb shift is due to the contribution of several multipolar modes and the fact that the dipole approximation to model the response of the nanoparticle (corresponding to the red curve in Fig. 1) fails to account for the Lamb shift. In other words, in the near-field region, the atom couples to several plasmon modes of the silver nanoparticle (see also [27]), which gives rise to the complex pattern of the Lamb shift spectrum.

In order to account for the spectral line shape, we will make use of the analytical expressions of the dipolar and quadrupolar contributions derived in Appendix VII B, in the case of a radially oriented dipole. In the non-retarded regime $kd \ll 1$ (which is fulfilled here), the analytical expression of the dipolar contribution ($n = 1$) reduces to,

$$\frac{\Delta\omega_1^{\perp}}{\gamma_0} = \frac{9}{2} \frac{1}{(kd)^6} \mathrm{Im}[a_1] + O\left((kd)^{-6}\right) \ , \qquad (16)$$

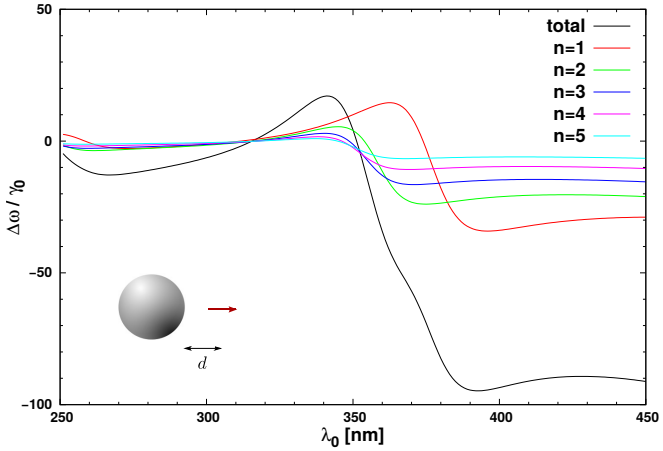

FIG. 1. Numerical simulations of the total Lamb shift $\Delta\omega$ (black curve) and its multipolar contributions $n = 1, 2, 3, 4, 5$ (colored curves) as a function of the transition wavelength $\lambda_0 = 2\pi c/\omega_0$ for a perfect electric dipole emitter with radial orientation and located at $d = 10\,\text{nm}$ from a silver nanosphere with $a = 20\,\text{nm}$ radius (red arrow). The Lamb shift is normalized to the dipole's decay rate in free space γ_0. The refractive index of the homogeneous background is $n_b = 1$. A Drude-Lorentz model for the silver permittivity is used according to [28]. The total Lamb shift is computed by taking $n_{\text{cut}} = 10$.

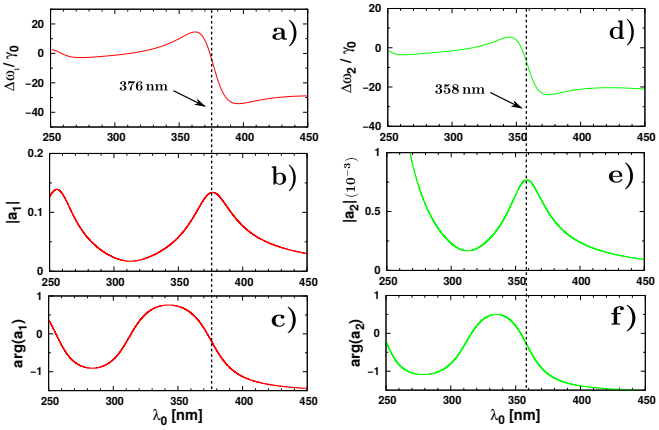

FIG. 2. (a) and (d): Lamb shift dipolar (red curve) and quadrupolar (green curve) contributions of Fig.1 (same color code) normalized by γ_0. (b) and (e): Modulus of the associated electric dipolar (red curve) and quadrupolar (green curve) Mie coefficients a_1 and a_2 as a function of the excitation wavelength λ_0. (c) and (f): Argument of the associated electric dipolar (red curve) and quadrupolar (green curve) Mie coefficients a_1 and a_2 as a function of λ_0. A Drude-Lorentz model for the silver permittivity is used according to [28].

while the quadrupolar contribution ($n = 2$) reduces to,

$$\frac{\Delta\omega_2^{\perp}}{\gamma_0} = \frac{405}{2}\frac{1}{(kd)^8}\text{Im}[a_2] + O\left((kd)^{-8}\right) , \qquad (17)$$

where the subscript $\perp$ indicates a dipole perpendicular to the particle surface (radially oriented), and a_1 (a_2) is the electric dipolar (quadrupolar) Mie coefficient whose expression can be found in Appendix VII A. The explanation of the spectral behavior of the Lamb shift is thus found in the imaginary part of the Mie coefficient. In Fig. 2, we plot the modulus ((b) and (e)) and phase ((c) and (f)) of the electric dipolar and quadrupolar Mie coefficients a_1 and a_2 respectively as a function of the excitation wavelength, together with the first two multipolar contributions $n = 1$ and $n = 2$ of Fig. 1 ((a) and (d) in Fig. 2 plotted with the same color code). One can see that the inflection point of the Lamb shift spectrum (around 376 nm for $n = 1$ and 358 nm for $n = 2$) corresponds to a resonance maximum of the modulus of the associated Mie coefficient accompanied by a strong phase change (the resonance of the Mie coefficients around 250 nm is a spurious resonance peculiar to the model of permittivity used [29]). This clearly shows the multipolar origin of the plasmon resonance enhanced Lamb shift.

B. Quasi-normal mode description

Another interpretation of the shape of the Lamb shift spectrum can be given using a Quasi-Normal Mode (QNM) description [30] (also called "Resonant State" expansions). By expanding the scattered field $\mathbf{E}_s(\mathbf{r}_0, \omega_0)$ in Eq. (4) onto a small set of QNMs of the plasmonic resonator as in [31], we obtain:

$$\left.\frac{\Delta\omega}{\gamma_0}\right|_{\omega_0} \simeq \sum_\alpha A_\alpha \left(\frac{\omega'_\alpha}{\omega_0}\right)^2 \frac{\omega''_\alpha}{2}\frac{\omega'_\alpha - \omega_0}{(\omega'_\alpha - \omega_0)^2 + \omega''^2_\alpha} + B_\alpha(\omega_0) , \qquad (18)$$

where $\omega_\alpha = \omega'_\alpha + \text{i}\,\omega''_\alpha$ is the complex frequency of the QNM labeled α, while A_α is a dimensionless factor and $B_\alpha(\omega_0)$ a function of ω_0 (for the qualitative analysis which follows, we will consider it as constant: $B_\alpha(\omega_0) \equiv B_\alpha$). An equivalent expression in term of the wavelength is obtained by extending the relation between ω and λ to complex numbers. Adopting $\lambda_\alpha \equiv 2\pi c/\omega_\alpha$, where $\lambda_\alpha = \lambda'_\alpha + \text{i}\,\lambda''_\alpha$ is the complex wavelength associated with the complex frequency, $\omega_\alpha = \omega'_\alpha + \text{i}\,\omega''_\alpha$, we find:

$$\left.\frac{\Delta\omega}{\gamma_0}\right|_{\lambda_0} \simeq \sum_\alpha -A_\alpha \left(\frac{\lambda'_\alpha}{\widetilde{\lambda}_0}\right)^2 \frac{\lambda''_\alpha}{2}\frac{\lambda'_\alpha - \widetilde{\lambda}_0}{(\lambda'_\alpha - \widetilde{\lambda}_0)^2 + \lambda''^2_\alpha} + B_\alpha , \qquad (19)$$

where $\widetilde{\lambda}_0 \equiv |\lambda_\alpha|^2/\lambda_0$. Note that Eqs. (18) and (19) are generally valid for any resonator shape, and shows that the total Lamb shift can be given by the sum of independent contributions of the QNMs.

For a spherical Mie resonator, the QNMs are the multipolar modes, labeled by three numbers $\{q, n, m\}$, whose associated complex eigenfrequencies $\omega_{q,n,m}$ are the poles of the Mie coefficients [32]. In order to find the QNM resonances in play in the previous configuration, we only look at the poles of the *electric* Mie coefficients, because the dipole emitter is radially oriented and therefore only couples to *electric* modes (see discussion at the end of Appendix VII B). This consists in solving the transcen-

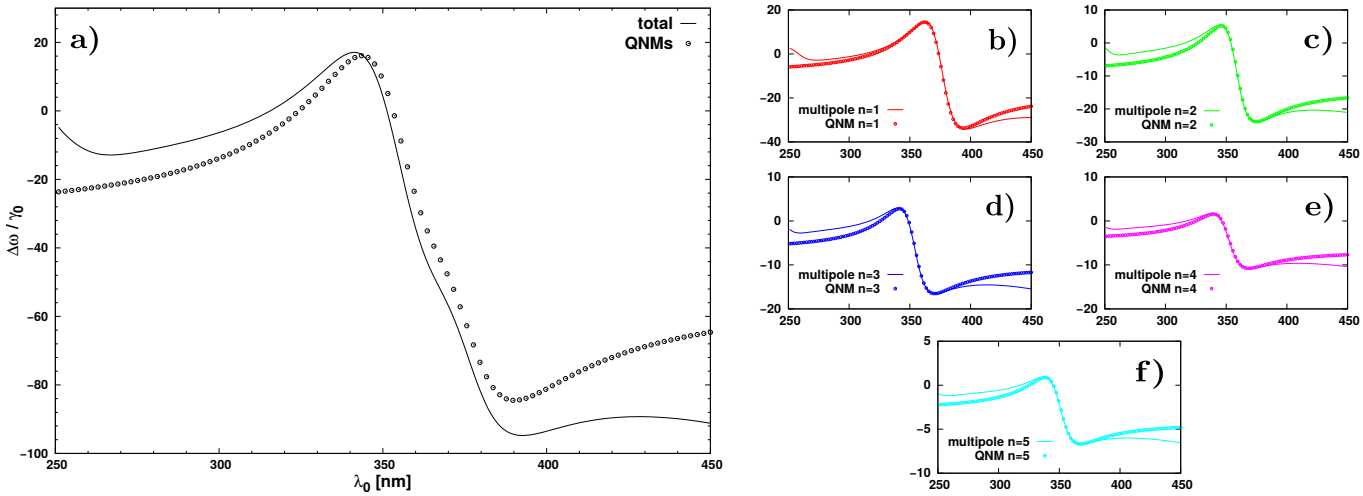

FIG. 3. Comparison between numerical simulations and analytical calculations of the Lamb shift. (a): Total Lamb shift of Fig. 1 (black curve) compared to the Lamb shift calculated with Eq. (21) using the five QNM resonances displayed in Table I (dotted curve). (b) to (f): Fit of each multipole contribution of Fig. 1 (full lines, same color code) with the corresponding QNM contribution calculated with Eq. (21) (dotted lines) with A_n and B_n the fitting parameters (displayed in Table I).

dental equation (see Eq. (A1)):

$$(\varepsilon_s/\varepsilon_b) j_n(k_s a)\xi_n'(ka) = \psi_n'(k_s a) h_n(ka) \ , \qquad (20)$$

where all the functions and parameters are defined in Appendix VII A. First note that Eq. (20) does not depend on m, which means that multipolar modes with the same multipolar order n but different orbital number m are degenerate (*i.e.* have the same eigenfrequency ω_n). Therefore, the Lamb shift in Eq. (19) can be expressed as a sum running on the multipolar order n,

$$\left.\frac{\Delta\omega}{\gamma_0}\right|_{\lambda_0} \simeq \sum_n -A_n \left(\frac{\lambda_n'}{\widetilde{\lambda}_0}\right)^2 \frac{\lambda_n''}{2} \frac{\lambda_n' - \widetilde{\lambda}_0}{(\lambda_n' - \widetilde{\lambda}_0)^2 + \lambda_n''^2} + B_n \ . \qquad (21)$$

For each n, we find one solution ω_n of Eq. (20) corresponding to the dominant pole, whose associated complex wavelength λ_n is given in Table I for $n = [1;5]$ (we still take the same Drude-Lorentz model for the permittivity of the silver nanosphere [28] as for the previous numerical simulations). The corresponding A_n and B_n terms are left as free parameters and they are set by fitting each multipole contribution n of Fig. 1 with the formula $-A_n \left(\frac{\lambda_n'}{\widetilde{\lambda}_0}\right)^2 \frac{\lambda_n''}{2} \frac{\lambda_n' - \widetilde{\lambda}_0}{(\lambda_n' - \widetilde{\lambda}_0)^2 + \lambda_n''^2} + B_n$, in Fig. 3 (b)-(f). The discrepancy out of resonance that can be seen in Fig. 3 (b)-(f) is due to the fact that Eq. (18) is valid only in the vicinity of the resonance frequencies ω_α and that we ignored the ω_0 dependency of B_α. The values of the A_n and B_n parameters that result from the fit are given in Table I for $n = [1;5]$. Note that the value of the amplitude A_n decreases as n increases, showing that the resultant coupling between the emitter and the QNM resonance n is less and less important.

In Fig. 3 (a), we compare the Lamb shift given by Eq. (21) using the five QNM resonances $n = [1;5]$ with the previous total Lamb shift calculated by computing Eq. (15) (black curve in Fig. 1). We can see that the analytical formula Eq. (21) based on the QNM resonances of the plasmonic resonator qualitatively reproduces the Lamb shift resonance when only a few dominant resonances are taken into account, but the convergence could be further improved by increasing the number of QNM resonances (see also [33, 34] where it is shown that a few set of QNM resonances is enough to reproduce the scattering properties of a particle). Moreover, this simple analytical formula clearly evidences that the Lamb shift resonance results from the coupling of the quantum emitter to the resonant modes of the nanoparticle.

Finally, it is interesting to note that this resonant coupling induces a *positive* Lamb shift $\Delta\omega = \omega - \omega_0 > 0$ (around 340 nm in the configuration under study, see Fig. 1 or Fig. 3 (a)), which was first predicted in the case of silver [9] and sodium [10] surfaces (see also [15] where a similar effect was reported in the case of a dielectric microsphere). This positive Lamb shift leads to a *repulsive van der Waals potential* as long as the atom remains in its excited state, which was shown experimentally with *excited* cesium atoms in the presence of a sapphire surface [35, 36].

TABLE I. **QNM complex wavelengths and fitting parameters.**

n	λ_n(nm)	A_n	B_n
1	$375.6 + 15.5\mathrm{i}$	95.7	−7.6
2	$358.2 + 14.0\mathrm{i}$	57.8	−8.2
3	$353.7 + 14.1\mathrm{i}$	38.3	−6.1
4	$351.7 + 14.2\mathrm{i}$	24.5	−4.1
5	$350.5 + 14.2\mathrm{i}$	15.0	−2.6

V. PREDICTIONS ABOUT THE LAMB SHIFT

A. Blue-shift of the resonance

In this section, we show how the size of the nanoparticle affects the position of the Lamb shift resonance. We still consider the case of a silver nanosphere. We plot in Fig. 4 the normalized Lamb shift as a function of the transition wavelength for different particle radii (full lines). The asymptotic case of a planar surface is also plotted (dashed line) according to the following expression [9, 10]:

$$\frac{\Delta\omega^{\perp}}{\gamma_0} = -\frac{3}{16k^3}\,\frac{|\varepsilon_s|^2-1}{|\varepsilon_s+1|^2}\,\frac{1}{d^3}\,, \tag{22}$$

which is valid in the non-retarded regime and for an emitter oriented perpendicular to the surface. In this case, the dipole emitter couples to the surface plasmon mode which comes from the infinite density of states of the high order modes (around $\lambda_0 \simeq 340\,\text{nm}$ for a planar silver surface).

In sharp contrast with a nanosphere characterized by a purely dipolar response, we predict in the near-field of the nanosphere a *blue*-shift of the Lamb shift resonance as the radius of the nanosphere increases (see Fig. 4). To understand this feature, let us recall that as the radius increases, each plasmon resonance is red-shifted and the dipole emitter couples to higher-order multipoles [27]. The displacement (blue-shift) of the Lamb shift resonance then results from the *interference* between these different modes. Therefore, this effect will only exist if the dipole emitter is located in the near-field of the nanoparticle, so that it will be able to excite *several* modes and to get this interference effect, resulting then in a blue-shift of the resonance.

Thus, it can be observed in Fig. 4 that in the near-field of the nanoparticle, a precise engineering of this resonant coupling between the quantum emitter and the plasmon resonances is possible. For instance, the transition wavelength at which the Lamb shift is suppressed is $\lambda_0 = 363\,\text{nm} > \lambda_0 = 357\,\text{nm} > \lambda_0 = 350\,\text{nm} > \lambda_0 = 342\,\text{nm} > \lambda_0 = 339\,\text{nm}$ for the radii $a = 2.5\,\text{nm}$, $a = 5\,\text{nm}$, $a = 10\,\text{nm}$, $a = 50\,\text{nm}$ and the case of the planar silver surface respectively. The tuning of this interaction is of current interest [37, 38], and we suggest that thanks to their highly tunable optical properties, metallic nanoparticles can also be used to tune and shape the Lamb shift of a nearby quantum emitter through a control of their geometry, but also spatial organization and environment, which can all be investigated through Eq. (14).

B. Gold dimer nanoantenna

In order to make a realistic calculation of the Lamb shift, let us now consider a gold dimer with a dipole emitter located at the center of the nanogap. This configuration is now experimentally realizable using DNA templates [39, 40]. To compute the Lamb shift, we take the parameters corresponding to [41]: the nanoparticles radius is 40 nm, the nanogap is 6 nm, and the effective refractive index surrounding the nanoparticles is $n_{\text{eff}} = 1.5$; the fluorescent molecule is an *Alexa Fluor 647* dye, which presents an emission peak around $\lambda_0 = 670\,\text{nm}$ with 40 nm width; its total decay rate in the homogeneous solution is measured at $\gamma_0 = 2.63\,\text{ns}^{-1}$ [42].

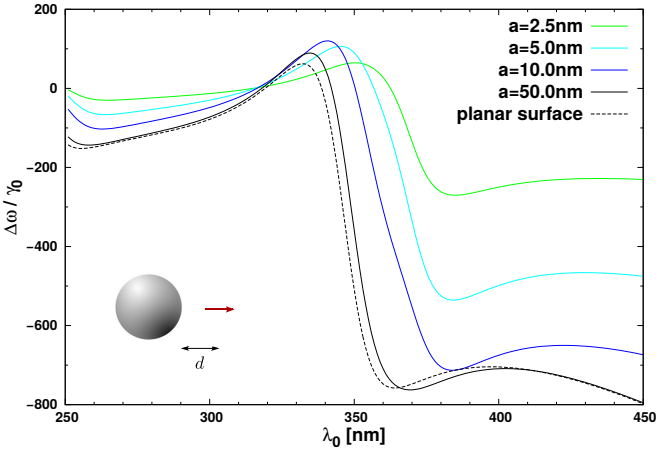

FIG. 4. Numerical simulations of the normalized Lamb shift $\Delta\omega/\gamma_0$ as a function of the transition wavelength λ_0 for a perfect electric dipole emitter with radial orientation and located at $d = 5\,\text{nm}$ from a silver nanosphere (red arrow), for different radii a (full lines). The asymptotic case of a planar silver surface (Eq. (22)) is also plotted (dashed line). The refractive index of the homogeneous background is $n_b = 1$. A Drude-Lorentz model for the silver permittivity is used according to [28]. The Lamb shift is computed by taking $n_{\text{cut}} = 10$ except for the case $a = 50\,\text{nm}$ where $n_{\text{cut}} = 50$ in order to converge.

The Lamb shift spectrum of such a configuration with a dipole emitter of parallel orientation is shown in Fig. 5. At $\lambda_0 = 670\,\text{nm}$, the normalized Lamb shift computed with Eq. (14) is $\Delta\omega/\gamma_0 = -8200$, which is *outside* of the range of the radiative linewidth, and therefore suitable for direct observation (the numerical simulations — not shown here — give a radiative decay rate enhancement $\gamma_r/\gamma_0 = 1700$ at $\lambda_0 = 670\,\text{nm}$). In order to find the Lamb shift of the dye, one needs to multiply the value given by the numerical simulations by the reference *quantum yield* $\phi_0 = 0.08$ in open solution (*i.e.* without the antenna): $\Delta\omega = \phi_0 \times (-8200) \times \gamma_0$. The corresponding shift in terms of wavelength is given by the following formula (valid if $\Delta\omega/\omega_0 \ll 1$): $\Delta\lambda/\lambda_0 = -\Delta\omega/\omega_0$ where $\Delta\lambda = \lambda - \lambda_0$ with λ the new wavelength of the emitted photon. Thus, for the Alexa Fluor 647 dye, the relative shift is $\Delta\lambda/\lambda_0 = 3.8 \times 10^{-3}$, corresponding to a shift $\Delta\lambda = 2.5\,\text{nm}$.

Such a shift could be detected at room temperature, by fitting the entire emission spectrum of the molecule (see for instance [43] where a shift of $\Delta\lambda \simeq 0.3\,\text{nm}$ has been detected — for the resonance spectrum of a gold nanorod — between neighboring Gaussian peaks with width of about 50 nm which is similar to our case here). One should also ensure that the spectral dependence of the Lamb shift, decay rate enhancement and quantum

yield enhancement, do not vary appreciably in the range used for fluorescence detection (the decay rate enhancement and quantum yield enhancement spectra for the same configuration can be found in [41], Fig. 3). In the future, it could be interesting to test the validity of the weak-coupling approximation to quantify the Lamb shift in such a configuration, by employing an other formalism suitable for investigating the strong-coupling regime such as the one presented in [44].

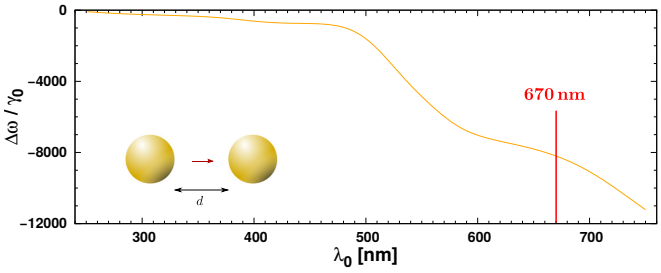

FIG. 5. Numerical simulations of the normalized Lamb shift $\Delta\omega/\gamma_0$ as a function of the transition wavelength λ_0 for a perfect electric dipole emitter with parallel orientation and located in the center of a gold dimer antenna of radius 40 nm and 6 nm gap (red arrow). The refractive index of the homogeneous background is $n_b = 1.5$. A Drude-Lorentz model for the gold permittivity is used according to [28]. The Lamb shift is computed by taking $n_{\text{cut}} = 40$.

VI. CONCLUSION

In this paper, we derived an exact multipole formula, Eq. (14), to compute the Lamb shift induced by an arbitrary set of resonant scatterers on a nearby quantum emitter. In the case of a single silver nanoparticle, our numerical simulations show that the dipole approximation fails to account for the total Lamb shift spectrum in the near-field region, and that one must include higher multipolar contributions. We furthermore adopted a Quasi-Normal Mode description of this phenomenon, which provides a more physically intuitive understanding of the induced Lamb shift as resulting from the coupling between the quantum emitter and the resonances of the nanoparticle, and shows that the total Lamb shift can be given by the sum of the independent resonance contributions. These formulas also predict a displacement of the Lamb shift resonance in the near-field to higher frequencies (blue-shift). Finally, a calculation of the Lamb shift in a physically realistic configuration indicates that a direct detection may be possible for fluorescent molecules embedded in a gold dimer nanogap.

VII. APPENDIX

A. Mie coefficients

In this Appendix, we give the expressions of the Mie coefficients in a slightly different way then in [45] (where they are called the scattering coefficients). By introducing ε_s (μ_s) and ε_b (μ_b) as the relative permittivity (permeability) of the sphere and the homogeneous background respectively, $k_s = \sqrt{\varepsilon_s(\omega)}\omega/c$ and $k = \sqrt{\varepsilon_b}\omega/c$, the Mie coefficients of a sphere of radius a take the form:

$$a_n = \frac{(\varepsilon_s/\varepsilon_b) j_n(k_s a)\psi_n'(ka) - \psi_n'(k_s a) j_n(ka)}{(\varepsilon_s/\varepsilon_b) j_n(k_s a)\xi_n'(ka) - \psi_n'(k_s a) h_n(ka)} \tag{A1}$$

for the electric Mie coefficient of order n, and

$$b_n = \frac{(\mu_s/\mu_b) j_n(k_s a)\psi_n'(ka) - \psi_n'(k_s a) j_n(ka)}{(\mu_s/\mu_b) j_n(k_s a)\xi_n'(ka) - \psi_n'(k_s a) h_n(ka)} \tag{A2}$$

for the magnetic Mie coefficient of order n, where $j_n(x)$ and $h_n(x)$ are respectively the spherical Bessel functions and the first-type (outgoing) spherical Hankel functions, and $\psi_n(x)$ and $\xi_n(x)$ are the Ricatti-Bessel functions defined as:

$$\psi_n(x) \equiv x j_n(x) \tag{A3}$$

$$\xi_n(x) \equiv x h_n(x)\ . \tag{A4}$$

B. Analytical expressions of the dipolar and quadrupolar Lamb shift

In this Appendix, we derive from Eq. (15) analytical expressions for the Lamb shift dipolar and quadrupolar contributions for a sphere. We consider the sphere placed in the $+z$ direction with respect to an electric dipole emitter oriented either perpendicular to the surface of the sphere (orbital number $m = 0$, dipole moment oriented on the z axis) or parallel to the surface ($m = 1$, dipole moment oriented on the x axis). Due to spherical symmetry, the T-Matrix of the single sphere is a diagonal matrix t composed of the Mie coefficients of the sphere multiplied by -1. With a quadrupolar assumption [46]:

$$t = -\text{Diag}(a_1, a_2, b_1, b_2)\ , \tag{B1}$$

with a_1 (a_2) the electric dipolar (quadrupolar) Mie coefficient and b_1 (b_2) the magnetic dipolar (quadrupolar) Mie coefficient defined in Appendix VII A,

$$f = [e_1, 0, 0, 0]^t\ , \tag{B2}$$

with e_1 the incident electric dipole coefficient, and

$$H^{(0,1)} = \begin{bmatrix} A_{1,m,1,m} & A_{1,m,2,m} & B_{1,m,1,m} & B_{1,m,2,m} \\ A_{1,m,2,m} & A_{2,m,2,m} & B_{1,m,2,m} & B_{2,m,2,m} \\ B_{1,m,1,m} & B_{1,m,2,m} & A_{1,m,1,m} & A_{1,m,2,m} \\ B_{1,m,2,m} & B_{2,m,2,m} & A_{1,m,2,m} & A_{2,m,2,m} \end{bmatrix}\ , \tag{B3}$$

where $A_{n,m,n',m'}$ ($B_{n,m,n',m'}$) the coupling coefficient from the electric (magnetic) multipole order n with orbital number m, to the multipole order n' with orbital number m'. Note that $H^{(1,0)}$ is the same as $H^{(0,1)}$ with all the B coefficients multiplied by -1. Employing the expressions of the coefficients A and B calculated in [46] in Eq. (15), one gets for an electric dipole oriented perpendicular to the particle surface ($m = 0$):

$$\frac{\Delta\omega_1^{\perp}}{\gamma_0} = \frac{9}{2}\mathrm{Im}\left[a_1 \frac{e^{2\mathrm{i}kd}}{(kd)^6}(1-\mathrm{i}kd)^2\right] \tag{B4}$$

for the dipolar contribution and

$$\frac{\Delta\omega_2^{\perp}}{\gamma_0} = -\frac{9}{10}\mathrm{Im}\left[a_2 \frac{e^{2\mathrm{i}kd}}{(kd)^8}\left(-15\mathrm{i}-15(kd)-25(kd)^2\right)^2\right] \tag{B5}$$

for the quadrupolar contribution. In the case of an electric dipole emitter oriented parallel to the particle surface ($m = 1$), the dipolar and quadrupolar contributions to the Lamb shift read:

$$\begin{aligned}\frac{\Delta\omega_1^{\parallel}}{\gamma_0} =& \frac{9}{8}\mathrm{Im}\left[a_1 \frac{e^{2\mathrm{i}kd}}{(kd)^6}\left(1-2\mathrm{i}(kd)-3(kd)^2+2\mathrm{i}(kd)^3+(kd)^4\right)\right] \\ &- \frac{9}{8}\mathrm{Im}\left[b_1 \frac{e^{2\mathrm{i}kd}}{(kd)^4}\left(\mathrm{i}+(kd)\right)^2\right]\end{aligned} \tag{B6}$$

$$\begin{aligned}\frac{\Delta\omega_2^{\parallel}}{\gamma_0} =& -\frac{15}{8}\mathrm{Im}\left[a_2 \frac{e^{2\mathrm{i}kd}}{(kd)^8}\left(6\mathrm{i}+6(kd)-3\mathrm{i}(kd)^2-(kd)^3\right)^2\right] \\ &+ \frac{15}{8}\mathrm{Im}\left[b_2 \frac{e^{2\mathrm{i}kd}}{(kd)^6}\left(3-3\mathrm{i}(kd)-(kd)^2\right)^2\right]\end{aligned} \tag{B7}$$

It is interesting to note in the case of a dipole emitter with parallel orientation the presence of the magnetic Mie coefficients b_1 and b_2, which traduce the cross-coupling between the electric dipole emitter and the magnetic multipole resonances. This is not the case for a dipole perpendicularly oriented whose multipolar Lamb shift contributions only depends on the electric Mie coefficients, since the magnetic field produced by an electric dipole is null along the dipole axis.

ACKNOWLEDGEMENTS

The authors want to thank Rémi Colom, Mahmoud Elsawy, Mauricio Garcia-Vergara, Xavier Zambrana-Puyalto and Jérôme Wenger for fruitful discussions. E. L. would like to thank the Doctoral School "Physique et Sciences de la Matière" (ED 352) for its respective funding.

[1] M. S. Tame, K. McEnery, Ş. Özdemir, J. Lee, S. Maier, and M. Kim, Nature Physics **9**, 329 (2013).
[2] E. M. Purcell, Physical Review **69**, 681 (1946).
[3] R. G. Hulet, E. S. Hilfer, and D. Kleppner, Physical review letters **55**, 2137 (1985).
[4] P. K. Jha, X. Ni, C. Wu, Y. Wang, and X. Zhang, Phys. Rev. Lett. **115**, 025501 (2015).
[5] D. Bouchet, M. Mivelle, J. Proust, B. Gallas, I. Ozerov, M. F. Garcia-Parajo, A. Gulinatti, I. Rech, Y. De Wilde, N. Bonod, V. Krachmalnicoff, and S. Bidault, Phys. Rev. Applied **6**, 064016 (2016).
[6] W. E. Lamb and R. C. Retherford, Phys. Rev. **72**, 241 (1947).
[7] H. A. Bethe, Physical Review **72**, 339 (1947).
[8] G. Barton, Journal of Physics B: Atomic and Molecular Physics **7**, 2134 (1974).
[9] R. R. Chance, A. Prock, and R. Silbey, Phys. Rev. A **12**, 1448 (1975).
[10] J. M. Wylie and J. E. Sipe, Phys. Rev. A **32**, 2030 (1985).
[11] A. Kofman, G. Kurizki, and B. Sherman, Journal of Modern Optics **41**, 353 (1994).
[12] S.-Y. Zhu, Y. Yang, H. Chen, H. Zheng, and M. S. Zubairy, Phys. Rev. Lett. **84**, 2136 (2000).
[13] X.-H. Wang, Y. S. Kivshar, and B.-Y. Gu, Phys. Rev. Lett. **93**, 073901 (2004).
[14] S. C. Ching, H. M. Lai, and K. Young, JOSA B **4**, 2004 (1987).
[15] V. V. Klimov, M. Ducloy, and V. S. Letokhov, journal of modern optics **43**, 2251 (1996).
[16] H. T. Dung, L. Knöll, and D.-G. Welsch, Phys. Rev. A **64**, 013804 (2001).
[17] V. Klimov, M. Ducloy, and V. Letokhov, The European Physical Journal D-Atomic, Molecular, Optical and Plasma Physics **20**, 133 (2002).
[18] A. Asatryan, L. Botten, N. Nicorovici, R. McPhedran, and C. M. de Sterke, Waves in Random and Complex Media **16**, 151 (2006).
[19] B. Stout, J.-C. Auger, and J. Lafait, Journal of Modern Optics **49**, 2129 (2002), http://dx.doi.org/10.1080/09500340210124450.
[20] B. Stout, J.-C. Auger, and A. Devilez, JOSA A **25**, 2549 (2008).
[21] W. Zhu, R. Esteban, A. G. Borisov, J. J. Baumberg, P. Nordlander, H. J. Lezec, J. Aizpurua, and K. B. Crozier, Nature communications **7** (2016).

[22] L. Novotny and B. Hecht, *Principles of nano-optics* (Cambridge university press, 2012).

[23] H. T. Dung, L. Knöll, and D.-G. Welsch, Phys. Rev. A **57**, 3931 (1998).

[24] S. Scheel, L. Knöll, and D.-G. Welsch, Phys. Rev. A **58**, 700 (1998).

[25] B. Stout, A. Devilez, B. Rolly, and N. Bonod, JOSA B **28**, 1213 (2011).

[26] X. Zambrana-Puyalto, Ph.D. thesis, Macquarie University (2014).

[27] G. C. des Francs, A. Bouhelier, E. Finot, J. C. Weeber, A. Dereux, C. Girard, and E. Dujardin, Opt. Express **16**, 17654 (2008).

[28] A. D. Rakić, A. B. Djurišić, J. M. Elazar, and M. L. Majewski, Applied optics **37**, 5271 (1998).

[29] F. Hao and P. Nordlander, Chemical Physics Letters **446**, 115 (2007).

[30] C. Sauvan, J. P. Hugonin, I. S. Maksymov, and P. Lalanne, Phys. Rev. Lett. **110**, 237401 (2013).

[31] J. Yang, M. Perrin, and P. Lalanne, Physical Review X **5**, 021008 (2015).

[32] X. Zambrana-Puyalto and N. Bonod, Physical Review B **91**, 195422 (2015).

[33] V. Grigoriev, A. Tahri, S. Varault, B. Rolly, B. Stout, J. Wenger, and N. Bonod, Phys. Rev. A **88**, 011803 (2013).

[34] S. Bakhti, N. Destouches, and A. V. Tishchenko, Journal of Quantitative Spectroscopy and Radiative Transfer **146**, 113 (2014), electromagnetic and Light Scattering by Nonspherical Particles {XIV}.

[35] M. Fichet, F. Schuller, D. Bloch, and M. Ducloy, Phys. Rev. A **51**, 1553 (1995).

[36] H. Failache, S. Saltiel, M. Fichet, D. Bloch, and M. Ducloy, Phys. Rev. Lett. **83**, 5467 (1999).

[37] S. A. Aljunid, E. A. Chan, G. Adamo, M. Ducloy, D. Wilkowski, and N. I. Zheludev, Nano letters **16**, 3137 (2016).

[38] E. A. Chan, S. A. Aljunid, G. Adamo, A. Laliotis, M. Ducloy, and D. Wilkowski, arXiv preprint arXiv:1606.07990 (2016).

[39] M. P. Busson, B. Rolly, B. Stout, N. Bonod, and S. Bidault, Nature communications **3**, 962 (2012).

[40] S. Bidault, A. Devilez, V. Maillard, L. Lermusiaux, J.-M. Guigner, N. Bonod, and J. Wenger, ACS nano **10**, 4806 (2016).

[41] D. Punj, R. Regmi, A. Devilez, R. Plauchu, S. B. Moparthi, B. Stout, N. Bonod, H. Rigneault, and J. Wenger, ACS photonics **2**, 1099 (2015).

[42] R. Regmi, A. A. Al Balushi, H. Rigneault, R. Gordon, and J. Wenger, Scientific reports **5** (2015).

[43] I. Ament, J. Prasad, A. Henkel, S. Schmachtel, and C. Sönnichsen, Nano letters **12**, 1092 (2012).

[44] H. Varguet, B. Rousseaux, D. Dzsotjan, H. R. Jauslin, S. Guérin, and G. C. des Francs, Opt. Lett. **41**, 4480 (2016).

[45] C. F. Bohren and D. R. Huffman, *Absorption and scattering of light by small particles* (John Wiley & Sons, 2008).

[46] B. Rolly, B. Bebey, S. Bidault, B. Stout, and N. Bonod, Physical Review B **85**, 245432 (2012).